Mapping of Peroxyl Radical Induced Damage on Genomic DNA†

Henry Rodriguez,‡ Michael R. Valentine,§ Gerald P. Holmquist,§ S. A. Akman,|| and John Termini*,§

Division of Biology, Beckman Research Institute of the City of Hope, 1450 East Duarte Road, Duarte, California 91010, DNA Technologies Group, Biotechnology Division, NIST, 100 Bureau Drive, Mail stop 8311, Gaithersburg, Maryland 20899, and Department of Cancer Biology, Comprehensive Cancer Center of Wake Forest, Medical Center Boulevard, Winston-Salem, North Carolina 27157

Received August 13, 1999; Revised Manuscript Received October 13, 1999

ABSTRACT: We have examined the DNA damage produced by reaction of peroxyl radicals with human fibroblast DNA. DNA damage consisted of both strand breaks and base modifications. The extent of strand breaks and base modifications induced as a function of peroxyl radical concentration was determined by quantitation of fragment size distributions using denaturing glyoxal-agarose gel electrophoresis. Both strand breaks and base modifications increased in a log linear fashion with respect to peroxyl radical concentration. Oxidative base modifications were observed to occur to a greater extent than strand breaks at every concentration measured. The sequence-specific distribution of peroxyl radical induced base damage was mapped for 803 nucleotide positions using the method of ligation mediated PCR. A total of 87% of all guanine positions in the examined sequences was found to be significantly oxidized. The order of reactivity of DNA bases toward oxidation by peroxyl radicals was found to be G ≫ C > T. Adenine is essentially unreactive. The yield of oxidative base modifications at guanines and cytosines by peroxyl radicals depends on the exact specification of 5′ and 3′ flanking bases in a polarity dependent manner. Every guanine in the 5′X*G*C3′ motif was found to be oxidized, where X is any 5′ neighbor. In contrast, 5′ and 3′ purine flanks drastically reduced the extent of peroxyl radical *G* oxidation. The pattern of base modification and the influence of nearest neighbors differs substantially from that previously reported for hydrogen peroxide damage mediated by low valent transition metal ions for the identical DNA sequences.

Many endogenous oxidative processes may give rise to peroxyl radicals (ROO•)[1] under physiological conditions. The reaction of carbon radicals (R•) with oxygen generates peroxyl radicals at a nearly diffusion controlled rate (*1*). Carbon radicals of any biomolecule may be formed via the abstraction of an H atom by oxidizing species; the addition of a radical such as (•OH) to double bonds; and by the direct action of ionizing radiation. Peroxyl radicals are remarkable owing to their extremely long half-life ($\tau_{1/2} \approx 0.5-2.0$ s), which endows them with considerable potential for diffusion in biological media (*2*). The stability of peroxyl radicals relative to other oxygen radicals also suggests greater chemical selectivity. This is exemplified by the preferred abstraction of bis-allyic methylene hydrogens over mono-allylic hydrogens by peroxyl radicals during the propagation phase of lipid peroxidation (*9*). Although peroxyl radicals have been most thoroughly studied within the context of membrane autoxidation, where they are the main-chain carrying radical (*4*), peroxyl radicals of amino acids (*5*, *6*) and DNA (*2*, *3*, *7*, *8*) have also been characterized.

Peroxidation of membrane lipids has been implicated in the etiology of human cancers (*10*, *11*). The realization that dietary intake of polyunsaturated fats can alter the composition of organellar membranes provides a molecular link between dietary modification and the enhanced risk for biological damage (*12*−*15*). Increased levels of polyunsaturated lipids has been suggested to be a risk factor in cancer owing to genetic damage which may occur as a result of peroxidation. Peroxidation occurring within the nuclear membrane is of special concern.

There are two main pathways by which DNA damage by lipid peroxidation may occur. Radical intermediates generated during the course of lipid peroxidation undergo free radical chain terminating decomposition events to generate electrophilic aldehydes such as glyoxal (*16*); 2,3-epoxy-hydroxynonanal (*17*, *18*); and malondialdehyde (*19*). These compounds are known to react with DNA to form base adducts, and the mutagenicity of the resulting lesions and their endogenous distribution are highly active areas of research. Distinct from this alkylative pathway of DNA damage is the oxidative DNA damage that is incurred as a direct result of the reaction of DNA with long-lived peroxyl radicals. Little is known about the products resulting from

† This work was supported by PHS Grants GM53962 and GM59219 (J.T.) and CA69449 (G.H.).

* To whom correspondence should be addressed. Phone: (626) 301-8169. Fax: (626) 301-8271. Email: jtermini@smtplink.coh.org.

‡ DNA Technologies Group.

§ Beckman Research Institute of the City of Hope.

|| Comprehensive Cancer Center of Wake Forest.

[1] Abbreviations: AP, apurinic/apyrimidinic PCR, polymerase chain reaction; LMPCR, ligation-mediated polymerase chain reaction; PGK, phosphoglycerate kinase; EDTA, ethylenediaminetetraacetic acid; SDS, sodium dodecyl sulfate; DMEM, Delbucco's Minimum Essential Media; DMSO, dimethyl sulfoxide; AAPH, 2, 2′-azobis-(2-methylpropionamidine)-dihydrochloride; DTT, dithiothreitol; BSA, bovine serum albumin; BER, base excision repair; Fpg, Formamido pyrimidine glycosylase; Nth, endonuclease III; HPLC-ESI-MS, high-performance liquid chromatography−electrospray ionization−mass spectroscopy; ROO•, alkyl peroxyl radical.

10.1021/bi9918994 CCC: $18.00
Published on Web 11/23/1999

the oxidation of DNA by peroxyl radicals and the mutagenic potential of such unrepaired damage. Peroxyl radicals resulting from reaction of DNA base radicals with oxygen [DNA(OO•)] have been implicated as intermediates in the generation of strand breaks (*2*, *3*). Thus, it appears that peroxidation of DNA can occur, although susceptible sites of oxidation analogous to the bis-allylic hydrogen positions of polyunsaturated lipids remain to be identified.

We have been studying the reaction products of DNA produced by reaction with peroxyl radicals and have recently reported on the mutation spectrum induced upon transfection of DNA oxidized by chemically generated ROO• (*20*). In *Escherichia coli*, an unusual pattern dominated exclusively by G → C and G → T transversions has been observed. Similar patterns have been obtained in related transfection assays using DNA exposed to peroxidizing liposomes (*21*). To determine whether the mutation pattern reflected highly specific reactivity of peroxyl radicals for guanine or a biased pattern of lesion repair deficient in repair of guanine damage, we decided to map DNA damage induced in vitro on genomic DNA oxidized by peroxyl radicals in a manner identical to that used to create DNA base damage in the mutational studies. Genomic DNA damage maps were constructed using DNA repair enzymes as reagents for the creation of strand breaks at oxidized bases. Break positions were then revealed using ligation-mediated PCR (LMPCR). This enabled us to create peroxyl radical damage maps for selected primer defined regions of two human genes (p53 and PGK1). Strong sequence context effects on the oxidation patterns were observed. These results were compared to the DNA damage patterns previously mapped for low valent transition metal ions and hydrogen peroxide along the same exon fragments (*22*).

EXPERIMENTAL PROCEDURES (MATERIALS AND METHODS)

Preparation of Fibroblast DNA. Human male fibroblasts were grown in 150 mm dishes to confluent monolayers in antibiotic-free Dulbecco's Modified Eagle Medium containing 10% (v:v) fetal bovine serum. Media was aspirated off and cells were rinsed with 15 mL of 1× PBS. This was repeated one time. Cells were then lysed by adding 10 mL of buffer A (0.3 M sucrose, 60 mM KCl, 15 mM NaCl, 60 mM Tris-HCl, pH 8.0, 0.5 mM spermidine, 0.15 mM spermine, and 2 mM EDTA) containing 0.5% Nonidet-P40 (ICN Biochemicals, Aurora, Ohio). Cells were immediately placed into a 50 mL polypropylene centrifuge tube on ice and incubated for 15 min. Nuclei were then sedimented by centrifugation (10 min/1000*g*/4 °C). Pelleted nuclei were then washed with 10 mL of buffer A. After centrifugation (10 min/1000*g*/4 °C), pelleted nuclei were resuspended in 5 mL of buffer B (150 mM NaCl and 5 mM EDTA, pH 8.0) and 5.7 mL of buffer C (20 mM Tris-HCl, pH 8.0, 20 mM NaCl, 20 mM EDTA, of 1% SDS). Proteinase K was added to achieve a final concentration of 600 μg/mL and the reactions were incubated for 3 h at 37 °C. Finally, RNase A was added to a final concentration of 100 μg/mL, and incubation was continued for an additional hour. DNA solutions were extracted twice with equilibrated phenol and once with chloroform. DNA was precipitated by addition of 200 mM NaCl and 2.5 vol of EtOH, allowed to stand for 5 min at room temperature, then centrifuged (30 min/1000*g*/4 °C). Supernatants were carefully removed, and pellets were washed once with 70% EtOH, then air-dried for 30 min. DNA was resuspended in 10 mM Hepes/1 mM EDTA and concentrations were determined spectrophotometrically (1 OD_{260} = 50 μg/mL).

Oxidation of Genomic DNA by Peroxyl Radicals. The diffusion-controlled reaction of carbon radicals generated by the thermal decomposition of a water soluble diazo compound with O_2 was used to generate peroxyl radicals. AAPH [2,2′-azobis(amidinopropane)hydrochloride] was obtained from the WAKO Chemical Co. (Tokyo, Japan). Solutions of genomic DNA (10 μg/500 μL) in doubly distilled deionized water were saturated with oxygen by bubbling 99.99% O_2 for 15 min at 4 °C through a glass capillary. Aliquots of freshly prepared stock solutions of AAPH (100 mM) were then added to DNA reactions to provide final concentrations over a range of 0.025−5.0 mM. Reactions were sealed and initiated by heating to 40 °C in an environmental incubator. After a reaction time of 1 h, DNA reactions were passed through a G-25 Sephadex spin column, and the DNA was precipitated as described above.

Quantitation of Peroxyl Radical Induced Strand Breaks in DNA. Precipitated peroxyl radical treated DNA was resuspended in 4.5 μL of ddd water, 2 μL of 100 mM sodium phosphate, pH 7.0, 10 μL DMSO, and 3.5 μL of 6 M glyoxal and incubated at 50 °C for 1 h. Glyoxal modification prevents rehybridization of DNA, allowing for analysis of the MW distribution of single-stranded fragments. Four microliters of loading dye (50% glycerol, 10 mM sodium phosphate, and 0.25% each bromphenol blue and xylene cyanol) was added, and the samples were immediately subjected to electrophoresis in 0.6% agarose 10 mM sodium phosphate pH 7 at 3−4 V/cm. A mixture of *Hae*III restricted ΦX-174 DNA and *Hin*dIII restricted λ DNA was used to calibrate the weight range of fragments as a function of migration distance in the gel. Gels were stained with 1 μg/mL acridine orange for 45 min and destained overnight in water. Fluorescent DNA bands were visualized with a Vista Fluorescence/Fluoroimager Si (Molecular Dynamics Inc., Sunnyvale, CA) using the Molecular Dynamics ImageQuant software. The intensity of the fluorescence is directly proportional to the number of fragments in a certain molecular weight range. Digitization of the fluorescent image for each lane was accomplished using Molecular Dynamics ImageQuaNT software. Each lane was divided into ∼1000 cells. From the digitized image data, the single-stranded DNA break distribution was determined by comparison to the size-mobility calibration curve obtained using the marker lane. The data for each lane (fragment distribution for a specified peroxyl radical dose) is then fitted to an equation which describes the idealized distribution predicted by random fragmentation theory (*23*):

$$w_t = tp^2 e^{-pt}$$

The variable w_t is the weight fraction of DNA found in segments of base pair length t, and p is the probability of a break. In practice, the integrated form of the equation is used:

$$W_X = 1 - (1 + pt)e^{-pt}$$

W_X is the weight fraction of cleaved DNA having a length

of less than or equal to *t*. This was determined by summing the fraction of the total pixel density for each cell from the bottom of the digitized image to the top (maximum length *t*). Plots of W_X vs log *t* were then constructed. By choosing an appropriate value of *p*, the data could be fitted to the equation. The value 1/*p* yields the break density. Thus for example, when 50 μM of AAPH was used to generate peroxyl radical induced breaks, the random break equation could be fitted with a *p* value of 0.000 19. This corresponds to a break density of 1 in 5300.

Quantitation of Peroxyl Radical Induced Base Modification in DNA. DNA base modifications were detected as breaks created by the combined DNA glycosylase/AP lyase activities of a mixture of base excision repair (BER) enzymes. The break densities were then determined using glyoxal gel electrophoresis as described above. Since the weight distributions represent the results of strand breaks caused by BER enzyme activity in addition to direct breaks caused by attack of peroxyl radicals on the DNA backbone, the data must be corrected in order to determine the base modification frequency. Thus $(1/p)_{ROO\cdot+BER} - (1/p)_{ROO\cdot} =$ base modification density. The base excision repair enzymes used as reagents in this work were the Fpg and Nth proteins, obtained from Dr. Timothy R. O'Connor of the Department of Biology, Beckman Research Institute of the City of Hope. The specific activities of the Fpg and Nth proteins were 3.0×10^4 and 2.5×10^4 units/mg, respectively. The specific activity of the Fpg protein was defined as picomoles of formamido-pyrimidine nucleotides released in 5 min from [^{3}H] Fapy-poly(dG-dC)•poly(dG-dC) as previously described (*24*). The activity of the Nth protein is defined as nanomoles of apurininc/apyrimidinic sites removed in 30 min using [^{3}H] AP DNA as a substrate (*25*). Purified human fibroblast DNA (1 μg) oxidized by peroxyl radicals was digested with 400 ng of Fpg and 100 ng of Nth in 50 mM Tris-HCl, pH 7.6, 100 mM KCl, 1 mM EDTA, pH 8.0, 0.1 mM DTT, and 500 μg/mL BSA. Reactions were carried out in a total volume of 100 μL for 1 h at 37 °C, then quenched by the addition of 250 μL of H_2O and 50 μL of 0.8% SDS. Reactions were then extracted two times with chloroform-saturated phenol and one time with chloroform. DNA was precipitated by the addition of 18 μL of 5 M NaCl and 1000 μL of EtOH, cooling on dry ice for 10 min, then centrifugation at 4000 rpm for 10 min. Supernatants were carefully decanted, and pellets were dried in a Speed-vac. Samples were then resuspended in the glyoxal containing loading buffer and analyzed as described above.

LMPCR Footprinting of Peroxyl Radical Induced Base Modifications. A concentration of peroxyl radicals equivalent to that used in the previously reported mutational studies (*20*) was used to generate DNA base modifications. Human fibroblast DNA (10 μg/500 μL) was treated with 100 μM of AAPH initiator in an O_2 saturated aqueous solution at 40 °C for 1 h. Samples were passed through a G-25 Sephadex column and precipitated and dried as described above. The DNA pellets were then resuspended in Sequenase buffer (40 mM Tris-HCl, pH 7.7, and 50 mM NaCl) and brought to a final concentration of 0.16 μg/μL in preparation for PCR analysis. The modified LMPCR protocol for the analysis of oxidative base damage in DNA has been described in detail (*26*). Key steps with recent enzyme modifications such as the incorporation of a hot start by using AmpliTaq Gold polymerase to provide better signal-to-noise ratio and cycling modifications are described below. The primers used for the analysis of PGK and p53 gene fragments are shown in Table 1. The procedure for the LMPCR detection of strand breaks produced by BER enzymes at modified bases consists of six steps: (1) hybridization of a gene-specific primer, Primer 1, followed by polymerase extension using Sequenase (U.S. Biochemicals, Cleveland, OH) up to the site of the break to generate a blunt end; (2) ligation of a double-strand linker via T4 DNA ligase; this requires a 5′ phosphate in addition to a blunt end. The DNA repair enzymes used to create strand breaks at the modified DNA bases generate 5′ phosphate ends; (3) PCR amplification (~20 cycles) was carried out using Primer 2 and a second primer complementary to the ligated universal primer; (4) separation of the amplified DNA fragments by polyacrylamide gel electrophoresis; (5) transfer of the DNA to a charged nylon membrane; (6) blotting with a radiolabeled probe (Primer 3) to produce a footprinting ladder.

Primer Extension. Reactions were carried out in a 0.65 mL tube. A thermocycler (MJ Research Inc., Watertown, MA) was used for all incubations. DNA (0.5−1.3 μg) was diluted in a volume of 15 μL of a solution containing 40 mM Tris-HCl, pH 7.7, 50 mM NaCl, and 0.75 pmol of Primer 1. DNA was denatured at 98 °C for 3 min and the primer (Primer 1) annealed at 45 °C for 30 min. After cooling the sample to 4 °C, 9 μL of the following mix was added: 7.5 μL of $MgCl_2$-dNTP mix (20 mM $MgCl_2$, 20 mM dithiothreitol, and 0.25 mM of each dNTP), 1.1 μL of dH_2O, and 0.4 μL o f Sequenase 2.0 (13 units/μL, U.S. Biochemicals, Cleveland, Ohio). Samples were then incubated at 48 °C for 15 min. The samples were placed on ice, and 6 μL of ice-cold 310 mM Tris-HCl, pH 7.7, was added. To inactivate Sequenase samples were incubated at 67 °C for 15 min.

Ligation. The primer-extended molecules that have a 5′ phosphate were ligated to an unphosphorylated asymmetric double-stranded linker. To each sample (consisting of 30 μL), 45 μL of the following ligation mix was added: 13.33 mM $MgCl_2$, 30 mM dithiothreitol, 1.7 mM ATP, 83.3 μg/mL BSA, 100 pmol of linker, and 5 units of T_4 DNA ligase (5 units/μL, Boehringer Mannheim, Gaithersburg, MD). Samples were incubated overnight at 18 °C. Ligase was inactivated by incubation at 70 °C for 10 min. DNA was precipitated by the addition of 25 μL of 10 M ammonium acetate, 1 μL of 0.5 M EDTA, pH 8.0, and 1 μL of 20 μg/μL glycogen, followed by 250 μL of ice-cold ethanol. DNA pellets were redissolved in 50 μL of dH_2O.

PCR Amplification. A total of 50 μL of an AmpliTaq Gold polymerase mix (2× AmpliTaq Gold reaction buffer) (Perkin-Elmer Inc., Foster City, CA), 1 mM $MgCl_2$, 400 FM of each dNTP, 10 pmol of primer 2, 10 pmol of linker primer, and 3.0 units of AmpliTaq Gold polymerase (5 units/μL, Perkin-Elmer Inc., Foster City, CA) were added to each sample, and reactions were overlaid with mineral oil. The final [Mg^{2+}] in the 100 μL reaction was 2 mM. Reactions were incubated at 95 °C for 16 min (activating AmpliTaq Gold polymerase). The PCR program consisted of 20 PCR cycles at 95 °C for 1 min, 1 °C below T_m of primer 2 for 2 min, and 72 °C for 3 min. The last step following the PCR cycles was an extension reaction, carried out at 72 °C for 3 min. Following the PCR reaction and extension, a stop mix (13 μL of 3 M sodium acetate, pH 5.2, 3 μL of 0.5 M EDTA,

Table 1: Primers Used in the Mapping of Peroxyl Radical Base Damage

primer set	sequence (5′ to 3′)	position[a]	T_m (°C)[b]
	PGK1		
transcribed strand			
A1	AAGTCGGGAAGGTTCCTT	−238 to −221	50
A2	AAGGTTCCTTGCGGTTCGCGGCG	−230 to −208	72
A3	CGGCGTGCCGGACGTGACAAAC	−212 to −191	70
G1	TCACGTCCGTTCGCAGC	−317 to −301	56
G2	CCGTTCGCAGCGTCACCCGGATC	−311 to −289	72
G3	GGATCTTCGCCGCTACCCTTGTG	−293 to −272	64
N1	CGGTGTTCCGCATTCTGC	−3 to +15	57
N2	TTCTGCAAGCCTCCGGAGCGCAC	+10 to +32	70
N3	GCACGTCGGCAGTCGGCTCCC	+29 to +49	70
nontranscribed strand			
D1	TTTGTCACGTCCGGCAC	−192 to −208	53
D2	ACGCCGCGAACCGCAAGGAACCT	−207 to −229	72
D3	CCGCAAGGAACCTTCCCGACTTA	−217 to −239	64
F1	CGTCCAGCTTGTCCAGC	+134 to +118	52
F2	TCCAGCGTCAGCTTGTTAGAAAGCG	+123 to + 99	64
F3	AGAAAGCGACATTTTGGAAATACAG	+106 to +85	56
H1	CCGGAGGCTTGCAGAAT	+25 to −9	53
H2	GCTTGCAGAATGCGGAACACCGCG	+19 to −5	72
H3	GCAGGAACAGGGCCCACACTAC	−9 to −30	61
	P53		
transcribed strand			
5-1	CACTTGTGCCCTGACTTTCAAC	+13009 to +13030	54
5-2	TGCCCTGACTTTCAACTCTGTCTCC	+13015 to +13039	60
5-3	CAACTCTGTCTCCTTCCTCTTCCTACAG	+13027 to +13054	58
9-1	GAGGAGACCAAGGGTGCAGT	+14615 to +14634	53
9-2	CCAAGGGTGCAGTTATGCCTCAGATTCA	+14622 to +14649	66
9-3	ATGCCTCAGATTCACTTTTATCACCTTTCC	+14636 to +14665	62

[a] Primer numbering is relative to transcription start site. [b] Melting points calculated using the Oligo 4.0 program. Definitions of nested primers 1−3 are provided in the Materials and Methods.

pH 8.0, and 9 μL of dH_2O) was added under the mineral oil layer. Samples were extracted with 170 μL of premixed phenol:chloroform (50 μL:120 μL), then ethanol precipitated by adding 370 μL of ice-cold ethanol. Air-dried DNA pellets were dissolved in 7.0 μL of premixed formamide-dye [2.3 μL of dH_2O, 4.7 μL of formamide loading dye: 95% (v/v) formamide, 10 mM EDTA, pH 8, 0.05% (w/v) xylene cyanol, and 0.05% (w/v) bromophenol blue] in preparation for sequencing gel electrophoresis.

Electroblotting and LMPCR Signal Detection. The amplified fragments were separated on a 30 × 40 cm 8% polyacrylamide/7M urea sequencing gel. The DNA was then transferred to a charged nylon membrane (Qiabrane, Qiagen, Chatsworth, CA) using the HEP3 electroblotting apparatus (Owl Separation Systems, Portsmouth, NH) for 45 min at 2 A, 15 V. The sample was then UV cross-linked to the membrane (1000 J/m^2) using a Stratalinker 2400 (Stratagene). Signal was by hybridization of a third gene specific probe (Primer 3) to the membrane. Hybridization was performed using a Hoefer (San Francisco, CA) hybridization oven in an 80 mm × 20 cm borosilicate hybridization tube at a temperature which was 2 °C below the T_m of Primer 3 for 12 h. Membranes were then washed for 10 min with buffer I (20 mM sodium phosphate, pH 7.2, 1 mM EDTA, 2.5% SDS, 0.25% BSA, and then three times with buffer II (20 mM sodium phosphate, pH 7.2, 1 mM EDTA, and 1% SDS) 30 min. each.

Quantitative Analysis of Autoradiographic Data. DNA bands were visualized, digitized and integrated using a PhosphorImager equipped with ImageQuant software (Molecular Dynamics). The intensities of each band were normalized to the corresponding signals obtained by Maxam−Gilbert chemical sequencing reactions (*27*) of untreated fibroblast DNA. The bands corresponding to the sequencing lanes were generated by LMPCR using the same protocol and corresponding primer sets applied to the peroxyl radical treated DNA. The band intensities for each base position created by Maxam−Gilbert cleavage were assigned an arbitrary signal intensity of 1. The intensity values of the bands generated by peroxyl radical base oxidation were divided by the intensities of the corresponding Maxam−Gilbert bands, and values of ≥1 were plotted as histograms for all positions within the primer sets. The peroxyl radical induced base "hits" exhibited intensities up to five times the Maxam−Gilbert signal intensities. This normalization procedure allowed correction for nonlinear variations in the ligation and amplification steps for the determination of the relative extent of base modification. Data for 803 base positions, corresponding to eight primer sets, were analyzed in this manner. The influence of flanking bases on the frequency of modification by peroxyl radicals was analyzed statistically for all four bases. Only the influence of immediate 5′ and 3′ neighbors was examined (base triplets).

Statistical Methods. Statistical analyses were carried out by Dr. Jeffrey Longmate, Department of Research Statistics, Beckman Research Institute of the City of Hope. Likelihood-ratio tests from log-linear models were used to test variation across bases and primer-defined regions. Four models for neighboring base effects were evaluated: null, additive, symmetric, and full context. The effect of flanking bases was

shown to be dependent on orientation ($p = 0.003$), ruling out a symmetric model. The residual deviance statistic, which measures lack of fit, is reduced by 31% when the full context model is used to predict the base modification frequencies. The improvement is comprised of contributions from additive effects for each purine or pyrimidine at neighboring positions (21%), and 10% by specific combinations of 5′ and 3′ bases.

RESULTS

Peroxyl Radical Oxidation of DNA Produces Both Strand Breaks and Base Modifications. Peroxyl radicals may be considered to be radiomimetic in the sense that exposure to DNA produces both strand breaks and base modifications. To quantitate the relative contributions of each to the DNA damage profile, glyoxal denaturing gel electrophoresis was used extensively. Since glyoxal prevents renaturing of double-stranded DNA by irreversibly modifying purines (predominantly adenine), analysis on agarose gels at neutral pH provides information on the size distribution of single-stranded fragments. The data analysis used to derive break density values is essentially identical to that utilized in the classical technique of alkaline elution of irradiated and chemically treated DNA in cells (*28*, *29*). Since some types of DNA damage lesions are alkali labile leading to strand breaks (*30*), the use of alkaline elution for the present studies would likely overestimate the density of direct single-strand breaks, a situation obviated by the use of glyoxal denaturant at neutral pH. Quantitation of strand breaks induced by proteins of the DNA glycosylase/AP lyase family was used to provide a measure of the extent of base modification induced by peroxyl radicals, after subtracting the break density resulting from direct oxidation of the DNA backbone. A typical glyoxal-agarose gel result used in the quantitation of peroxyl radical induced strand breaks and base modifications is shown in Figure 1. Comparison of lanes 1 and 2 reveals the extent of DNA damage in the untreated sample. This corresponds to the background oxidative base damage and apurinic/apyrimidinic sites that are detectable by a combination of Nth and Fpg proteins. Correction for this inherent background was accomplished by subtracting the break density value obtained from lane 2 (0.2 breaks/10 kb) from all peroxyl radical oxidized DNA samples subsequently treated with Nth and Fpg proteins. Lanes 3 and 4 of Figure 1 show the distribution of single-stranded fragments and base modifications resulting from exposure of fibroblast DNA to 100 μM AAPH in O_2 saturated aqueous solution for 1 h.

The substrate range for most of the known DNA glycosylases/AP lyases appears broad (*31*) and has not yet been completely defined for any member of this family. A mixture of these enzymes is used in order to ensure that the widest possible extent of DNA damage is detected. Enzymes are used in large excess in these experiments in order to help overcome possible differences in the apparent second-order rate constants (k_{cat}/K_M) which may occur for particular types of base damage within different sequence contexts. Analysis of break densities using data such as that shown in Figure 1 over a range of peroxyl radical concentrations allows for the construction of the break density curves compiled in Figure 2.

Concentrations of peroxyl radical were estimated using the relation described by Niki (*32*). The data of Figure 2 shows that base modifications (■) dominate the DNA damage spectrum. The increase in base modifications as a

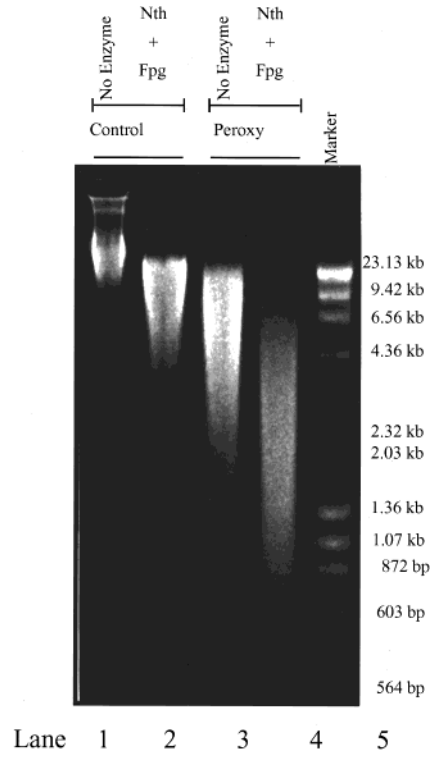

FIGURE 1: Glyoxal-agarose gel electrophoretic analysis of peroxyl radical induced strand breaks and base modifications. Break density determinations were obtained from the integrated gel data as described in Materials and Methods. Lane 2 reveals the extent of the background base modifications present in human fibroblast DNA as Nth and Fpg protein induced strand breaks (0.2 breaks/kilobase) of unoxidized DNA. Lanes 3 and 4 correspond to peroxyl radical treated samples (100 μM AAPH/O_2, 1 h). The integrated data of Lane 3 were used to quantitate single strand breaks induced by peroxyl radical. These break density values were used to correct integrated gel data obtained from peroxyl radical oxidized DNA after treatment with Nth and Fpg proteins (lane 4), which introduces additional strand breaks at modified bases. Corrected data yields the base modification frequency. Lane 5 is a marker lane used in size calibration.

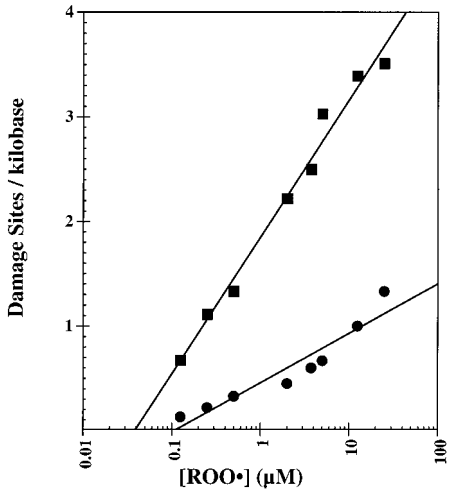

FIGURE 2: Dose dependence of strand breaks (●) and base modifications (■) induced by peroxyl radicals. Values were determined as described in Materials and Methods using glyoxal−agarose gel electrophoresis of fibroblast DNA oxidized by peroxyl radicals over a range of concentrations for 1 h at 37 °C. Concentrations of peroxyl radicals were calculated as described (*32*).

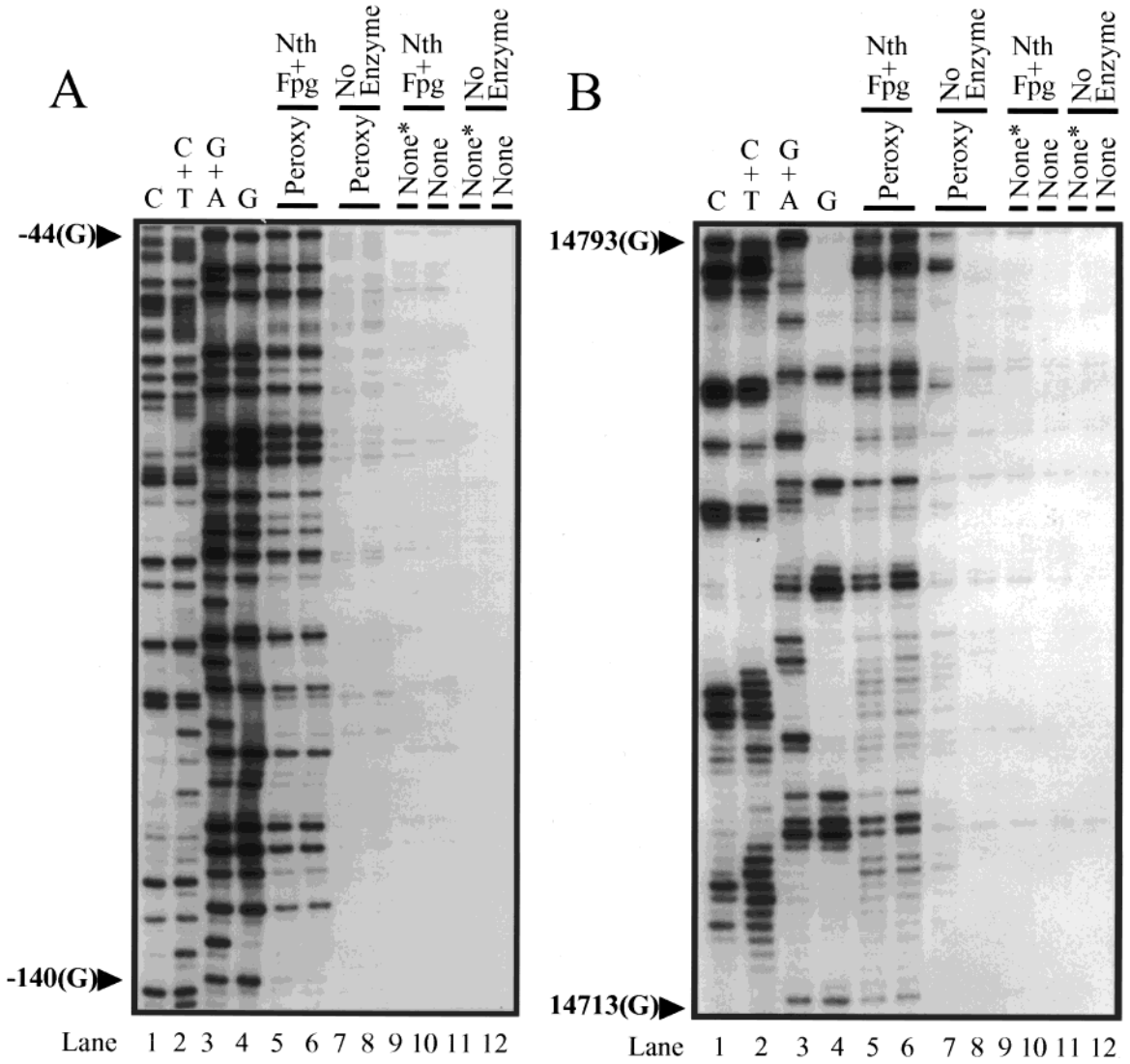

FIGURE 3: Representative autoradiograms of LMPCR data of peroxyl radical induced DNA base damage for panel A, PGK1 primer set A, and (B) the p53 exon 9 primer set. For both panels A and B: lanes 1−4, Maxam−Gilbert sequencing data of genomic DNA generated by LMPCR following chemical treatment. Lanes 5 and 6, peroxyl radical oxidized DNA reacted with Fpg and Nth proteins prior to LMPCR mapping. Lanes 7 and 8, LMPCR signals DNA damage histograms derived from LMPCR data resulting from peroxyl radical oxidized DNA without enzyme digestion. Lanes 9 and 10, unoxidized DNA treated with Fpg + Nth proteins. Lanes 11 and 12, pattern obtained from mapping untreated control fibroblast DNA.

function of peroxyl radical concentration is log linear ($r^2 = 0.98$) over the range of concentrations examined. Similar behavior is obtained for peroxyl radical induced strand breaks (●), with a slightly lower correlation coefficient ($r^2 = 0.90$). The base modifications occur on average 4.7 ± 1.2 times more frequently than strand breaks.

Sequence-Specific Determination of Peroxyl Radical Induced Base Modifications by LMPCR. A total of 803 nucleotide positions consisting of fragments of the human p53 and PGK1 genes was analyzed for peroxyl radical induced base damage. Conditions of oxidation were identical to that previously described for the determination of the peroxyl radical induced mutation spectrum (*20*). Gene segments analyzed are defined from the 3′ side by the primers listed in Table 1. The methodology allows for the analysis of ~120 bases downstream from primer 1. Both transcribed and untranscribed strands of the PGK1 gene were examined, while only transcribed regions of p53 exons 5 and 9 were studied. Although there was significant variation between primer-defined regions, no apparent correlation with transcription status on the base modification frequency was observed.

Typical examples of the LMPCR data are shown in Figure 3 for regions corresponding to segments of the PGK1 gene and p53 exon 9, panels A and B, respectively. Lanes 1−4 are LMPCR-generated Maxam−Gilbert sequencing lanes. All other experiments were done in duplicate in order to enhance the accuracy of signal quantitation. Lanes 7 and 8 of Figure 3, panels A and B, demonstrate the weak-banding pattern obtained when peroxyl radical treated fibroblast DNA is subjected to LMPCR without prior digestion by BER enzymes. The weak signals obtained likely correspond to DNA fragments produced by peroxyl radical induced strand breaks. Since the T4 DNA ligase reaction of the LMPCR procedure requires a 5′ phosphate end, fragments detected in lanes 7 and 8 must possess this feature. The exact nature of the ends produced by peroxyl radical strand scission are currently unknown, but this result suggests that at least some fraction of the ends consist of 5′ phosphate. Peroxyl radical induced strand breaks which result in destruction of the

Table 2: Distribution of Peroxyl Radical Induced Base Modifications

primer set	% total damage[a]	% A[b]	% C	% G	% T
p53 Exon 5	43	13	12	85	11
p53 Exon 9	13	0	6	36	0
PGK A	30	0	5	100	6
PGK D	36	0	0	100	0
PGK F	36	9	6	100	0.0
PGK G	43	0	27	90	26
PGK H	41	0	9	85	0
PGK N	28	3	9	100	0

[a] Percentage of all bases within a primer defined region scored as peroxyl radical damaged bases. [b] % N refers to the percentage of N bases represented within a primer defined region modified by peroxyl radical.

terminal ribose and/or loss of 5′ phosphate cannot be detected by the LMPCR method. The extent of background base modification detected by LMPCR following treatment of unoxidized control DNA with Fpg and Nth proteins (lanes 9−10) was found to be minimal (Figure 3, panels A and B, lanes 9 and 10). This is in general agreement with the low level of background base modifications revealed from denaturing glyoxal gel analysis of total fibroblast DNA (Figure 1, lane 2).

The patterns of peroxyl radical induced base modifications were determined from the data in lanes 5 and 6 of Figure 3. The signal intensities measured with the ImageQuant software for individual bands in each lane were first normalized relative to the total amount of radioactivity/lane. The intensities of each band in lanes 5 and 6 were assigned relative intensity values by dividing by the intensity of the corresponding Maxam−Gilbert band (lanes 1−4). In this manner, histograms were generated from the LMPCR data. Histogram data for four of the sequence regions examined is presented in Figure 4 (the complete set of histograms for all 803 bases analyzed is available as Supporting Information). There is considerable variability in the hit intensity levels. The relative intensities, which may be viewed as the extent of detectable base modification at a particular site, are observed to be strongest for guanines. Frequency of modification within a primer-defined region is highly variable. This is best illustrated by comparing the histograms for the analyzed regions of the p53 gene corresponding to exons 5 and 9. The overall hit frequency was observed to be lowest for exon 9, with relatively low intensities scored for modified bases. In contrast, exon 5 displayed one of the highest levels of base modifications within any of the gene segments examined, with 43% of base positions scoring as positive for modification by peroxyl radical. The base modification frequencies for all primer sets are provided in Table 2.

Base Modification by Peroxyl Radical Is Dominated by Reaction with Guanine. Examination of the data in Table 2 reveals an overwhelming preference for oxidation of guanine by peroxyl radical. Out of 803 base positions analyzed, 87% of all guanines was scored with intensities of ≥1. However, statistically significant variation in guanine modification frequency was found among different primer defined regions ($p < 0.000\,01$). Examination of Table 2 reveals that 100% of guanine positions the PGK A sequence was detected as peroxidized, whereas only 13% of guanines in the p53 exon 9 sequence was modified. The percentage of guanine in these sequences is similar; i.e., 26 and 33% G content in PGK A and p53 exon 9 respectively, yet peroxyl radical G oxidation is dramatically lower in the latter sequence. This suggests that the sequence context strongly influences oxidizability by peroxyl radical (see below).

Table 3: N Base Modification in 5′XNY3′ Base Triplets

X, Y	N = G[a]	intensity N = C[b]	G motif repeats[c]	N = C	C motif repeats
C, C	100	3.69	33	15	20
G, C	100	3.69	23	16	19
A, C	100	3.23	17	13	16
T, C	100	3.17	12	35	17
C, G	92	2.04	28	4	28
G, G	83	1.58	32	0	32
A, G	50	1.00	10	7	14
T, G	100	2.19	16	0	13
C, A	92	2.62	13	11	9
G, A	45	0.54	19	10	19
A, A	63	1.09	11	0	9
T, A	86	1.57	7	0	8
C, T	93	2.27	15	13	15
G, T	76	1.59	17	6	17
A, T	43	0.71	7	0	3
T, T	92	1.69	13	0	10

[a] Percentage of guanines with 5′ and 3′ neighbors X and Y detected as modified (intensity ≥ 1). [b] Mean hit intensity values for all N bases in an XNY motif. [c] Number of times a triplet motif occurs.

Adenines are oxidized rarely by peroxyl radicals (Table 2). Among pyrimidines, 9% of all cytosine positions were modified, nearly twice that detected for thymine. Cytosine modification was found to vary from 0 to 27% within specific primer defined regions. For the PGK G sequence, 8 of a possible 30 cytosine positions were found to be oxidized, whereas in the PGK D sequence, with 31 potential C target sites, none was found to be oxidized. Similar effects likely exist for oxidation at thymine; however, the small number of oxidized thymines makes a statistically meaningful nearest neighbor analysis difficult.

Nearest Neighbor Effects on Frequency and Intensity of Base Modification. The identity of 5′ and 3′ nearest neighbors on the pattern of base modification appears to dictate to a large degree the likelihood of oxidation as well as the intensity of the damage signal measured by LMPCR. These effects were explored in detail for base triplets only, i.e., the target base and the immediate 5′ and 3′ flanking bases. The extent of modification by peroxyl radicals as a function of nearest neighbor bases for guanine and cytosine is compiled in Table 3 (X, Y = 5′, 3′ flanking bases respectively). Mean intensity values for guanine damage sites are also presented. The most striking effect for oxidation at guanine (N = G) was observed when cytosine was the nearest 3′ neighbor, regardless of the 5′ flanking base (Table 3, rows 1−4). Guanines in this sequence context (N*G*C) were invariably oxidized by peroxyl radical.

In general, purine flanks lowered the susceptibility of guanines to oxidation by peroxyl radical, while pyrimidine flanks enhanced the reactivity (Table 3). Greater than 90% of all pyr*G*pyr sites was modified. Far lower levels of guanine modification were observed in motifs such as G*G*A (45%) and A*G*A (63%). A dramatic example of how these triplet motifs can influence reactivity of particular DNA sequences can be found by examining the peroxyl radical modification pattern within the p53 exon 9 sequence. Only 13% of

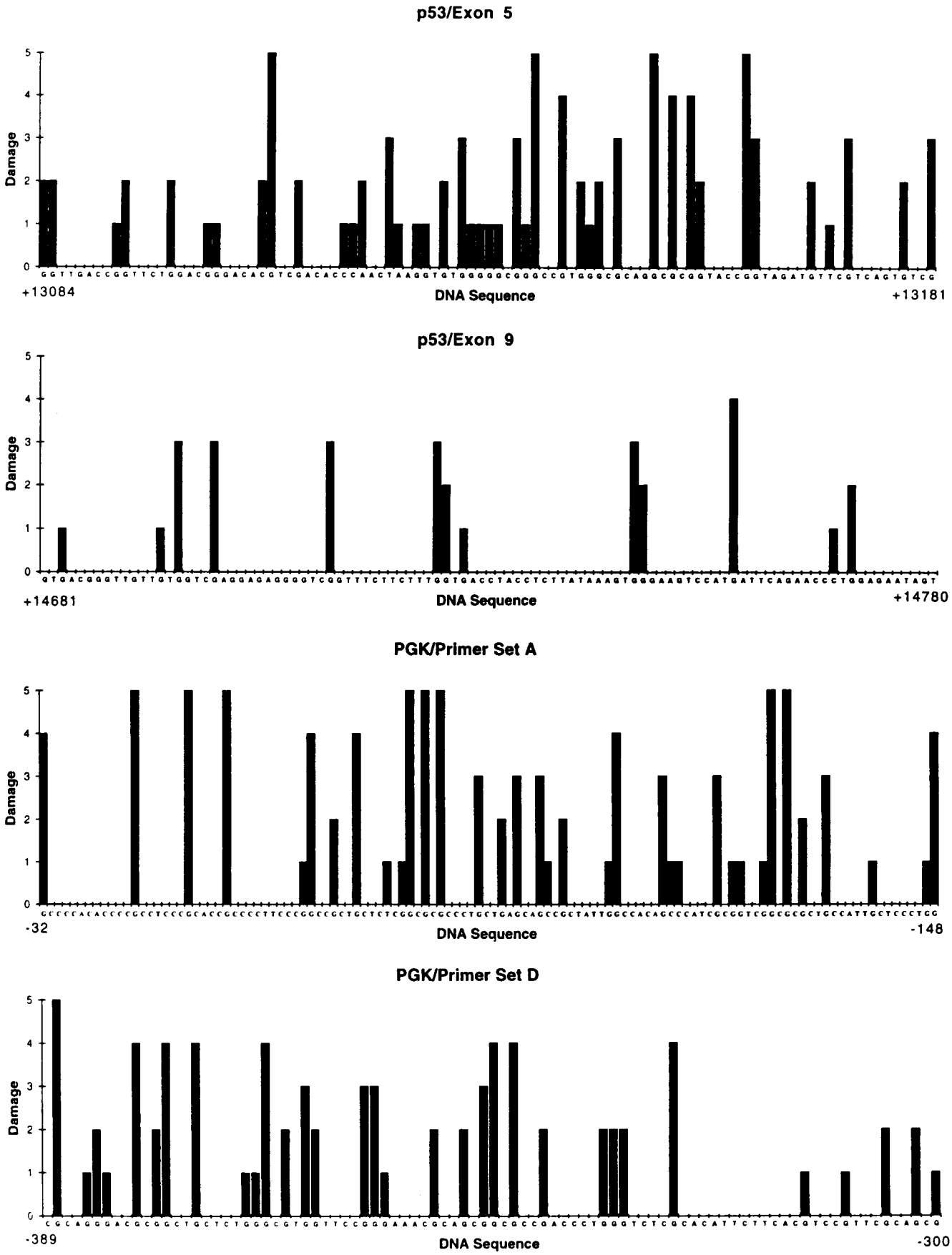

FIGURE 4: Histograms obtained from Phosphoimager analysis of LMPCR autoradiograms. Four out of eight primer set analyses are presented. The sequences defined by the respective primer sets, along with the numbering of the base positions within the indicated gene fragments, are also shown. Ordinate intensity values are defined arbitrarily from 0 to 5 based upon normalization to LMPCR amplified Maxam Gilbert lanes as described in the text.

guanines in the p53 exon 9 sequence was oxidized by peroxyl radical. Examining the nearest neighbors for all guanines reveals a total absence of the preferred N*G*C motif. Moreover, sequence motifs with lowered reactivity such as A*G*G (50%), G*G*A(45%), A*G*A (63%), A*G*T (43%), and G*G*T (76%) account for more than 50% of all guanines. These observations likely explain the very low levels of G modification observed within p53 exon 9.

The influence of flanking bases on oxidation appears to be asymmetric, i.e., switching the 5′ and 3′ orientation for a pair of flanking bases affects the oxidizability significantly ($p = 0.003$). For example, 100% of guanines in a T*G*G motif was detected as oxidized, whereas *G* oxidation drops to 76% in a G*G*T motif. Similar effects were observed for T*G*A and A*G*T sequence motifs, although these motifs occur relatively rarely in the analyzed sequences.

The relative intensity of modification, arbitrarily defined from 0 to 5, was similarly found to be dependent on the identity of the flanking bases. The highest measured intensities (mean values > 3) were observed for the N*G*C guanine motif. The intensity values provide additional information for ascertaining the susceptibility of certain sequence motifs toward oxidation. Thus, for example, while 83% of all *G* bases of the type G*G*G is detected as modified by peroxyl radical, the low mean intensity score (1.58) reveals that relative to guanines in more favorable motifs, the yield of detectable oxidation products is substantially lower. The lowest mean intensity value measured for guanines occurs in the G*G*A motif (0.54).

Although cytosine modification by peroxyl radical occurs far less frequently than reaction at guanine, some motifs are clearly favored. For example, 35% of *C* bases in T*C*C motifs were detected as oxidized, a level more than twice that for any other nearest neighbor configuration. Definitive conclusions about other motifs are difficult to make owing to an insufficient number of modified sites, but in general, where both 5′ and 3′ flanking bases are purines, cytosine modification is absent or present at a low level. Mean intensity data for cytosines are not recorded in Table 3, since all measured values were ≤2. The extent of detectable modification at thymine bases was too low for us to draw statistically meaningful conclusions about the effect of sequence context on oxidizability.

DISCUSSION

Mapping of peroxyl radical induced damage on genomic DNA for 803 base positions spanning several exons of unrelated gene sequences reveals a marked preference for guanine oxidation. Eighty seven percent of all guanines were detected as oxidized. This reactivity bias reflects the observed pattern of mutations found in *E. coli* forward mutation assays upon transfection of peroxyl radical oxidized plasmid DNA (*20*). Guanine is the most readily oxidized base (*33*), and the major product produced upon oxidation by either hydroxyl radicals (*34*) or singlet oxygen (*35*) is 8-hydroxyguanine. The oxidation of 2′-deoxyguanosine by peroxyl radicals, however, does not produce this well-studied oxidation product (20, *21*, *36*). The peroxyl radical mutation pattern is characterized by a large number of G → C transversions, a mutational event not associated with 8-oxoguanine base lesions in DNA (*37*, *38*). This transversion has also been observed in the Fe(II)/hydrogen peroxide induced mutation spectrum (*39*).

Table 4: Base Damage Induced by Fe(II), Cu(II), and Hydrogen Peroxide

primer set	% total damage[a,b]	% A[a,c]	% C[a,c]	% G[a,c]	% T[a,c]
p53 Exon 5	51	7	58	56	56
p53 Exon 9	55	62	47	61	50
PGK A	46	10	44	74	17
PGK F	51	0	61	62	13
PGK G	35	0	42	63	13

[a] Tabulated values calculated from data in ref *22*. [b] The percentage of all bases within the primer set that are scored as modified. [c] The percentage of the indicated base modified within the primer set.

Recently, it has been shown that an oxidation product resulting from the one electron oxidation and rearrangement of 8-oxo-guanine, possibly guanidinohydantoin, can give rise to G → C transversions (*40*). HPLC-ESI-MS analysis of peroxyl radical oxidation reactions of dG has failed to detect this product (J. Termini and D. C. Liebler, unpublished observations). This may suggest that additional, as yet uncharacterized, guanine oxidation products not derived from 8-oxoguanine can give rise to this transversion. Peroxyl radicals are also formed during the aerobic Fe(II)/hydrogen peroxide oxidation of DNA, although usually only hydroxyl radical damage is considered. We suggest that the G → C transversions observed in forward mutation assays of DNA treated in this manner could arise from the same guanine oxidation product(s) obtained in our studies.

Previously, the LMPCR lesion mapping methodology was used to determine the patterns of oxidative DNA modification caused by low valent transition metal ions [Fe(II), Cu(II)] and hydrogen peroxide (*22*). The base damage patterns for the iron and copper catalyzed reactions were observed to be identical. Four of the exon regions analyzed in this earlier work are identical to those presented here, thus direct comparison of the damage patterns is possible. Table 4 summarizes the data of Rodriguez et al. (*22*) for Fe(II)/Cu(II) catalyzed DNA damage by hydrogen peroxide. The total base damage detected for the hydrogen peroxide oxidations in each case is somewhat higher (mean value of 46% vs 33%) than for peroxyl radical reactions (Table 2). The base damage detected at cytosines and thymidines is substantially higher for the hydrogen peroxide reactions. Peroxyl radical oxidation of pyrimidines in contrast is a minor reaction (<10%).

It is interesting to note the nearly equivalent levels of C and T oxidation by peroxyl radicals within primer defined sequences. For example, the data for the primer set corresponding to PGK G in Table 2 reveals modification at C and T to the extent of 27 and 26%, respectively. A similar observation holds for the p53 Exon 5 data, where 12% of cytosines and 11% of thymidines are found to be modified. This may be rationalized in terms of the oxidizability of both substrates by peroxyl radicals. Peroxyl radicals react with thymidine by H atom abstraction at the C5 methyl group to provide a stabilized 5-yl radical (*41*). Sulfonyl peroxyl radicals have been shown to react in an identical fashion with thymidine (*42*). These reactions are analogous to the abstraction of bis-allylic hydrogens by lipid peroxyl radicals. The reaction pathway by which ROO· reacts with cytosine has not yet been determined. However, the NH bond

dissociation energies (BDE) of aromatic amines [~86−89 kcal/mol (*43*)] are similar to the BDE values calculated for the CH bond of thymine methyl [~ 85 kcal/mol (*42*)]. The energy required to break the N(4)H bond of cytosine could reasonably be expected to be within this range. Therefore, we suggest that since H atom abstraction at N(4)H of cytosine or C(5)H of thymine by peroxyl radicals is energetically nearly equivalent, oxidation of either base occurs with similar probability. The ROO−H bond dissociation energy has been estimated to be ~ 88−90 kcal/mol (*44*), thus peroxyl radical oxidation of aromatic amines is energetically feasible.

Effects of nearest neighbor bases on the frequency of guanine oxidation have been previously described for Type I photoreactions with DNA (*45*, *46*). Photoexcitation of a naphthalimide or riboflavin chromophore preferentially oxidized the central guanine in a G*G*G motif. Pyrimidine nearest neighbors were seen to adversely affect the oxidizability of guanines. In the peroxyl radical oxidation of guanine, 83% of all *G* bases in a G*G*G motif was found to be oxidized. Comparison with other triplet motifs in Table 3 clearly shows that this is not the most reactive arrangement for guanine oxidation by peroxyl radicals. Moreover, in contrast to the Type I photoreaction, guanines flanked by 3′ cytosines were determined to be preferred sites of oxidation by peroxyl radicals. The photosensitizaton reaction proceeds by initial $1e^-$ oxidation to produce the guanine radical cation. Electron rich nearest neighbors, optimally guanines, can greatly stabilize this intermediate in DNA (*47*).

It is not clear whether peroxyl radical oxidation of guanine takes place via initial radical cation formation. The preferred oxidation motif 5′X*G*C3′ suggests that it does not. If oxidation by ROO• takes place via H abstraction at N2 of guanine to yield a neutral amine radical, then the accessibility of this functional group to reactive oxidants in solution would be expected to influence the pattern of observed reactivity. Sequence-dependent DNA structure can lead to local variations in the disposition of base functional groups relative to the main helical axis. Calculations by Hunter have shown large variations in the relative relationship of stacked base pairs due to $\pi-\pi$ interactions (*48*). Dramatic differences are observed in the stacking geometry between 5′GC3′ and 5′CG3′ base pairs in B DNA. In the GC step, the energy minimum is characterized by a slide of −4 Å and a twist of 36°. This has the result of thrusting the guanine away from the center of the helix axis and out toward the minor groove. This places N2 of guanine in a solvent-accessible position toward the outer perimeter of the minor groove, favoring reaction. In contrast, the guanine of the CG step (slide = 2 Å, twist = 36°) lies close to the main helical axis, with N2 lying more deeply within the minor groove. This unusual orientation of guanine in the GC stack may also render the π electron system susceptible to addition by peroxyl radicals. This alternative mechanism is thermodynamically attractive.

The GC step is of special interest since among all possible $\pi-\pi$ stacking arrays it departs most radically from idealized B form helix geometry (*48*). This effect may be so large as to override any influence of the 5′ nearest neighbor on guanine oxidation, hence X*G*C is observed to be the preferred peroxyl radical oxidation motif. It will be of great interest to determine whether stacking "microheterogeneities" can account for some of the base triplet context effects reported in these studies. This would require extension of the approach of Hunter to three base pairs. The extent of $\pi-\pi$ overlap would depend on the precise specification of 5′ and 3′ nearest neighbors. This would not only result in "nonidealized" helical geometries for certain base combinations, but might also be expected to alter the ionization potentials of individual bases in DNA relative to their free nucleotide values.

SUPPORTING INFORMATION AVAILABLE

Complete set of histograms for all 803 bases analyzed. This material is available free of charge via the Internet at http://pubs.acs.org.

REFERENCES

1. Michaels, H. B., and Hunt, J. W. (1977) *Radiat. Res. 72*, 18−31.
2. Jones, G. D. D., and O'Neill, P. (1990) *Int. J. Radiat. Biol. 57*, 1123−1139; Hildebrand, K., and Schulte-Frohlinde, D. (1997) *Int. J. Radiat. Biol. 71*, 377−385.
3. Barvian, M. R., and Greenberg, M. M. (1997) *J. Am. Chem. Soc. 117*, 8291−8292.
4. Porter, N. A., Caldwell, S. E., and Mills, K. A. (1995) *Lipids 30*, 277−290.
5. Irwin, J. A., Ostdal, H., and Davies, M. J. (1999) *Arch Biochem. Biophys. 362*, 94−104.
6. Gebicki, S., and Gebicki, J. M. (1993) *Biochem. J. 289*, 743−749.
7. Deeble, D. J., and Von Sonntag, C. (1986) *Int. J. Radiat. Biol. 49*, 927−936.
8. Bothe, E., Behrens, G, Bohm, E., SethAuram, B., and Schulte-Frohlinde, D. (1986) *Int. J. Radiat. Biol. 49*, 57−66.
9. Wagner, B. A., Buettner, G. R., and Burns, C. P. (1994) *Biochemistry 33*, 4449−4453.
10. Welsch, C. W. (1995) *Free Radical Biol. Med. 18*, 757−773.
11. Sawa, T., Akaike, T., Kida, K., Fukushima, Y., Takagi, K., and Maeda, H. (1998) *Cancer Epidemiol., Biomarkers Prev. 7*, 1007−1012.
12. Tahin, Q. S., Blum, M., and Carafoli, E. (1981) *Eur. J. Biochem. 12*, 5−13.
13. Bourre, J. M., Bonneil, M., Nalbone, G., and Lafont, H. (1988) *Biochim. Biophys. Acta 960*, 458−461.
14. Bourre, J. M., Bonneil, M., Clement, M., Dumont, O., lafont, H., Nalbone, G., and Piciotti, M. (1993) *Prostaglandins, Leukotrienes Essent. Fatty Acids 48*, 5−15.
15. Stubbs, C. D., and Smith, A. D. (1984) *Biochim. Biophys. Acta. 779*, 89−137.
16. MLakar, A., and Spiteller, G. (1996) *Chem. Phys. Lipids 79* (1), 47−53.
17. Sodum, R. S., and Chung, F.-L. (1988) *Cancer Res. 320*−323.
18. El Ghissassi, F., Barbin, A., Nair, J., and Bartsch, H. (1995) *Chem. Res. Toxicol. 8*, 278−283.
19. Chaudhary, A. K., Nokubo, M., Reddy, G. R., Yeola, S. N., Morrow, J. D., Blair, L. A., and Marnett, L. J. (1994) *Science 265*, 1580−1582.
20. Valentine, M. R., Rodriguez, H., and Termini, J., (1998) *Biochemistry 37*, 7030−7038.
21. Akasaka, S., and Yamamoto, K. (1994) *Mutat. Res. 315*, 105−112.
22. Rodriguez, H., Holmquist, G. P., D'Agostino, R., Jr., Keller, J., and Akman, S. A. (1997) *Cancer Res. 57*, 2394−2403.
23. Montroll, E. W., and Simha, R. (1940) *Chem. Phys. 3*, 721−727.
24. Boiteux, S., O'Connor, T. R., Lederer, F., Gouyette, A., and Laval, J. (1990) *J. Biol. Chem. 265*, 3916−3922.
25. Cunningham, R. P., and Weiss, B. (1985) *Proc. Natl. Acad. Sci. 82*, 474−478.
26. Rodriguez, H., and Akman, S. A. (1998) *Free Radical Res. 29*, 499−510.
27. Maxam, A. M., and Gilbert, W. (1980) *Methods Enzymol. 65*, 499−560.

28. Kohn, K. W., Erickson, L. C., Ewig, R. A. G., and Friedman, C. A. (1976) *Biochemistry 15*, 4629−4637.
29. Nicolini C., Belmont, A., Zietz, S., Maura, A., Pino, A., Robbiano, L., and Brambilla, G. (1983) *J. Theor. Biol. 100*, 341−357.
30. Jones, A. S., Mian, A. M., and Walker, R. T. (1968) *J. Chem. Soc. C* 2042−2044.
31. Wallace, S. S. (1994) *Int. J. Radiat. Biol. 66*, 579−589
32. Niki, E. (1990) *Methods Enzymol. 186*, 100−108.
33. Steenken, S., and Jovanovic, S. V. (1997) *J. Am. Chem. Soc. 119*, 617−618.
34. Floyd, R. A., West, M. S., Eneff, K. L., Hogsett, W. E., and Tingey, D. T. (1988) *Arch. Biochem. Biophys. 262*, 266−272.
35. Devasagayam, T. P. A., Steenken, S., Obendorf, M. S. W., Schulz, W. A., and Sies, H. (1991) *Biochemistry 30*, 6283−6289.
36. Harkin, L. A., Butler, L. A., and Burcham, P. C. (1997) *Chem. Res. Toxicol. 10*, 575−581.
37. Moriya, M., Ou, C., Bodepudi, V., Johnson, F., Takeshita, M., and Grollman, A. P. (1991) *Mutat. Res. 254*, 281−288.
38. Cheng, K. C., Cahill, D. S., Kasai, H., Nishimura, S., and Loeb, L. A. (1992) *J. Biol. Chem. 267*, 166−172.
39. McBride, T. J., Preston, B. D., and Loeb, L. A. (1991) *Biochemistry 30*, 207−213.
40. Duarte, V., Muller, J. G., and Burrows, C. J. (1999) *Nucleic Acids Res. 27*, 496−502.
41. Martini, M., and Termini, J. (1997) *Chem. Res. Toxicol.* 10, 234−241.
42. Razskazovskii, Y., and Sevilla, M. D. (1996) *Intl. J. Radiat. Biol. 69*, 75−87.
43. MacFaul, P. A., Wayner, D. D. M., and Ingold, K. U. (1997) *J. Org. Chem., 62*, 3414−3414.
44. Jovanovic, S. V., Jankovic, I., and Josimovic (1992) *J. Am. Chem. Soc. 114*, 9018−9021.
45. Sugiyama, H., and Saito, I. (1996) *J. Am. Chem. Soc. 118*, 7063−7068.
46. Saito, I., Nakamura, T., Nakatani, K., Yoshioka, Y., Yamaguchi, K., and Sugiyama, H. (1998) *J. Am. Chem. Soc. 120*, 12686−12687.
47. Prat, F., Houk, K. N., and Foote C. (1998) *J. Am. Chem. Soc. 120*, 845−846.
48. Hunter, C. A. (1993) *J. Mol. Biol. 230*, 1025−1054.

BI9918994